

## XRD and SEM characteristics of Co-Ni ferrite nanoparticles Synthesized using sol-gel method

Sabah M. Ali Ridha<sup>1</sup>, Hussam A. Khader<sup>1</sup>

Department of physics/college of education for pure sciences/ University of Kirkuk, Kirkuk, Iraq.

Email: [sabahyagmur@uokirkuk.edu.iq](mailto:sabahyagmur@uokirkuk.edu.iq)

Email: [hussam0ahmed@gmail.com](mailto:hussam0ahmed@gmail.com)

Article history: Received, 30 July 2020, Revised, 15 January 2021, Accepted, 10 February 2021

### Abstract

Nickel-doped Cobalt ferrites nanoparticles (NPs) with chemical formula  $\text{Co}_{1-x}\text{Ni}_x\text{Fe}_2\text{O}_4$  (where,  $x = 0, 0.5, \text{ and } 1$ ) were synthesized at low temperature ( $200^\circ\text{C}$ ) using sol-gel autocombustion technique. Citric acid as a chelating agent used with the mixture of nickel nitrate and ferric nitrate solutions in a ratio of (3:1) to balance the oxidizing agent to reducer ratio. The obtained ferrite NPs were calcined at different temperatures (200, 400, 600, and  $800^\circ\text{C}$ ) for 4h in the air to remove the water content, unwanted impurities and to obtain a single-phase spinel structure with better crystallinity. Structural characteristics of the calcined ferrite NPs were confirmed by the analysis of the X-ray diffraction (XRD) technique. XRD analysis shows the single-phase cubic spinel nanocrystalline structure. The crystallite size calculated from FWHM of the strongest peak (311) is in the range of (27-44 nm) for  $\text{Co}_{1-x}\text{Ni}_x\text{Fe}_2\text{O}_4$  ferrite NPs. While, the  $\text{Co}_{0.5}\text{Ni}_{0.5}\text{Fe}_2\text{O}_4$  NPs have crystallite size larger than that of  $\text{NiFe}_2\text{O}_4$ , but smaller than  $\text{CoFe}_2\text{O}_4$  NPs. The lattice constant, X-ray density, and other structural parameters calculated from XRD data are in good agreement with the literature values. SEM images show NPs with spherical shape and homogenous morphology with particle size in the range of (25-47 nm), reflecting the highly crystalline nature of these nanoparticles. The average grain size of the samples obtained from SEM images is larger than the crystallite size calculated using XRD measurement, furthermore the distribution of the grains for Cobalt ferrite better than that of Nickel and Co-Ni ferrites. The particle size and grain size of the  $\text{Co}_{1-x}\text{Ni}_x\text{Fe}_2\text{O}_4$  ferrite NPs that calculated using XRD and SEM techniques are compatible with each other in the same range

**Keywords;** Co-Ni ferrite, SEM, Nanoparticles (NPs), sol-gel autocombustion, spinel ferrites, XRD

### Introduction

Ferrite nanoparticles (FNPs) an important branch within the group of magnetic nanoparticles (MNPs) and have received unlimited interest from researchers due to their unique properties and wide applications in electric and magnetic systems, high density information storage systems, magnetic cores, microwave devices absorbers, magnetic fluids, gas sensors, ferro-fluids, catalysts, and medical diagnostics, [1-10]. FNPs are composed of metal oxides with a cubic spinel structure and the general formula is  $\text{AB}_2\text{O}_4$ , ( $M = \text{Co, Mg, Mn, Ni, etc.}$ ). The metal cations A and B are located in two different crystalline sites known as the tetrahedral and octahedral sites respectively. Two cation metals are located at tetrahedral and octahedral sites to oxygen molecules. The unit cell of ferrite is contained 64 tetrahedral and 32 octahedral locations available for A and B cations, while only 8 tetrahedral and 24 octahedral sites are occupied by cations [11-12]. The arrangement of each type of the metal cations over the two sites depends on the ionic affinity of both sites, which in turn depends on the stability energy, the radius of the ions, and the method of preparation as well as the experimental conditions used in the preparation process [13-15]. The distribution of cations on the tetrahedral and octahedral sites has a significant effect on the physical and chemical properties of FNPs [16].

Cobalt ferrite ( $\text{CoFe}_2\text{O}_4$ ) is a spinel ferrite having cubic crystalline structure and known as a hard magnetic material with high coercivity and medium magnetization, which in turn makes it useful in the manufacture of high-density digital recording discs and audio/videotape [17]. On the other hand, cobalt ferrite has a high magnetocrystalline anisotropy, which makes it difficult to obtain high magnetic permeability [18]. Whereas, nickel ferrite is a soft magnetic material with low magnetic anisotropy, which provides a suitable and effective method to reduce the anisotropy of cobalt ferrite through the partial substitution of the  $\text{Co}^{+2}$  ion with a  $\text{Ni}^{+2}$  ion as in the formula  $\text{Co}_{1-x}\text{Ni}_x\text{Fe}_2\text{O}_4$  [19-20]. Many methods have been used to synthesize spinel ferrite nanoparticles such as hydrothermal method, sol-gel, co-precipitation, gel-assisted hydrothermal route, wet chemical co-precipitation technique, self-propagating. While the ferrite synthesized by the traditional ceramic method is used for specific applications as gas sensors due to the high-temperature processing of ferrite treatment in this method, which makes it a highly dense and

a small surface area [21-27].

The combustion reaction synthesis of ferrite powders is as other methods was used to prepare ceramic powders yields nanometric particles (< 100 nm) with high surface areas. The sol-gel autocombustion method is used to syntheses a range of mixed metal ferrite nanoparticles without decomposing the intermediate. The reason for using the autocombustion method is that it maintains the proportions of the components at the final product and thus assists the process of controlling the nanoparticles size of the product. In addition, this method possesses a number of advantages over other methods such as excellent mixing of starting materials, chemical homogeneity and purity of the final product, mixing at the molecular level and tendency of decomposing species to form extended networks, which in turn lowers the crystallization temperature [28]. The present work is concerned with the synthesis of nickel-substituted cobalt ferrite nanoparticles with the chemical formula  $Co_{1-x}Ni_xFe_2O_4$  (where  $x= 0, 0.5, \text{ and } 1.0$ ) via the sol-gel autocombustion method. The use of this method can produce a single-phase structure of ferrite nanoparticles. The structural and morphological properties of the ferrite nanoparticles can studied by using XRD and SEM analyses

**Experimental**

The Ni-Co ferrite nanoparticles having a composition of  $Co_{1-x}Ni_xFe_2O_4$  ( $x=0.0, 0.5, 1.0$ ) synthesized via the sol-gel auto combustion method. All the materials used in the preparation were AR grade with  $\square$  purity ( $\geq 99 \%$ ) bought from Sigma Aldrich. In the synthesis process, Iron nitrate  $Fe(NO_3)_3 \cdot 9H_2O$ , cobalt nitrate  $Co(NO_3)_2 \cdot 3H_2O$ , and nickel nitrate  $Ni(NO_3)_2 \cdot 6H_2O$  were used as oxidizing agents while citric acid used as fuel.

The metal nitrates and citric acid are weight in the required proportions; an appropriate amount of distilled water used to dissolve each compound separately by using a magnetic stirrer. After obtaining a clear solution for each compound, the metal nitrates mixed with a molar ratio for (Co+Ni) / Fe equal to (1:2) and then mixing the solution of metal nitrates and citric acid in a molar ratio of (1:1). Then, the final solution kept with constant stirring at  $80^\circ C$  on a magnetic stirrer. Ammonia solution was added dropwise to maintain  $pH = 7$  with constant stirring. This mixture heated at  $90^\circ C$  in order to convert into a gel.

This gel gradually heated by raising the temperature to about  $200^\circ C$  in order to ignite the gel and turn it into a fine loose powder, whereasthe resultant powder were collected and grounded. Depending on the decomposition pattern TG/DTA, all the resultant fine powders were calcined at deferent temperatures ( $200, 400, 600, \text{ and } 800^\circ C$ ) in a muffle furnace for 4 hour in order to get the nanocrystalline ferrite powders. This gel gradually heated by raising the temperature to about  $200^\circ C$  in order to ignite the gel and turn it into a fine loose powder, whereasthe resultant powder were collected and grounded. Depending on the decomposition pattern TG/DTA, all the resultant fine powders were calcined at deferent temperatures ( $200, 400, 600, \text{ and } 800^\circ C$ ) in a muffle furnace for 4 h in order to get the nanocrystalline ferrite powders to have a single-phase spinel structure with better crystallinity. Figure 1 shows a flow chart of the synthesis procedure leading to the formation of Co-Ni ferrite nanoparticles. A chemical reaction ( $Co_{1-x}Ni_xFe_2O_4$ ) stated as [29].

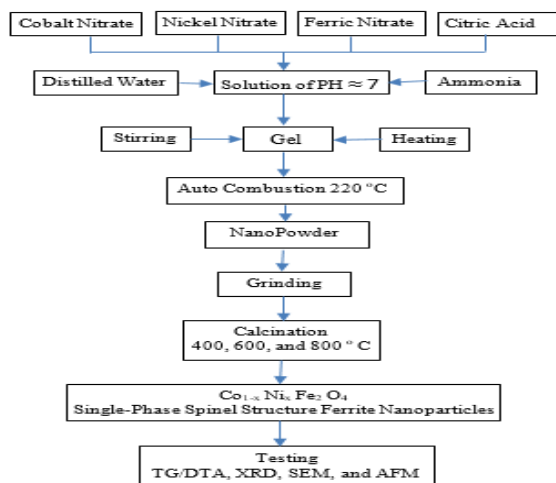
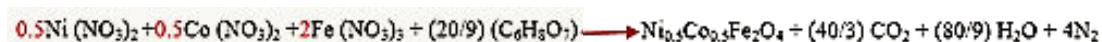


Figure 1: Flow chart of sol-gel autocombustion technique for Co-Ni spinel ferrite nanopowders.

## Result and Discussion

### Thermal Decomposition

The thermal decomposition, stability, and the temperature of phase formation study of Co-Ni ferrite powders with chemical composition of  $\text{Co}_{0.5}\text{Ni}_{0.5}\text{Fe}_2\text{O}_4$  (dried at 120 °C) is carried out by TGA-DTA. Figure (2) illustrates the relative weight variations associated with the entropy variations during the heating of the nano powders under air. Therefore, there is no weight increase observed, thus no oxidation process takes place under air for the prepared powder. Data is collected from the heating process at temperatures in the range of (25-1000 °C) with heating rate of 10 °C/min. The TGA curve shows 16% weight loss up to 180 °C, which corresponds to the evaporation of water molecules and volatile organic species as shown in Figure 2. A rapid decomposition has occurred between 180 to 300 °C due to the decomposition of polymeric species with a weight loss of 40%. Further decomposition is not observed beyond 300 °C, which specifies that the material is thermally stable in the temperature range of 300 – 1000 °C. DTA curve shows a broad endotherm in the temperature range of 100 – 300 °C with a small and narrow exothermic at 200 °C. The broad endotherm corresponds to the absorption of external heat to decompose the material, while a narrow exothermic represents crystallization of the complex organometallic compound. A broad exothermal observed between 400 – 700 °C attributes to the release of energy that can be used for the phase formation. The thermal decomposition and thermal stability from TGA-DTA curve can be well correlated to the XRD data for the investigations of phase transformation of samples annealed between 400 – 800 °C.

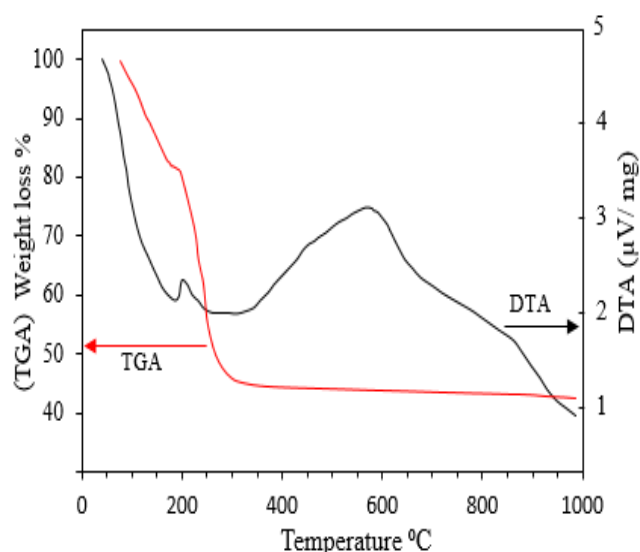


Figure 2: TGA-DTA, decomposition pattern of  $\text{Co}_{0.5}\text{Ni}_{0.5}\text{Fe}_2\text{O}_4$  (dried at 120 °C) ferrite gel.

### X-ray Diffraction Study (XRD)

The X-ray diffraction (XRD) patterns of  $\text{CoFe}_2\text{O}_4$ ,  $\text{NiFe}_2\text{O}_4$  and  $\text{Co}_{0.5}\text{Ni}_{0.5}\text{Fe}_2\text{O}_4$  ferrite nanopowders prepared by sol-gel method and then calcined at temperatures (22, 400, 600 and 800 °C) under atmospheric conditions for six hours holding time are shown in Figures 2, 3 and 4 respectively. The prominent Bragg reflections can be indexed as (111), (220), (311), (222), (400), (422), (511) and (440) planes of face centered cubic spinel type structure for all prepared ferrites.

Figure 3 illustrates that all peaks for cobalt ferrite calcined at different temperatures closely resemble the standard crystalline structure of  $\text{CoFe}_2\text{O}_4$  from (ICDD-221086), which belongs to face-centered cubic spinel-type (Fd-3m)

and there are no characteristic peaks indicating the presence of unexpected oxides or other impurities in the XRD patterns. The sample calcined at 800°C exhibits the highest intensity in comparison with the other samples.

In figure 4 and 5, the formation of  $\text{NiFe}_2\text{O}_4$  and  $\text{Co}_{0.5}\text{Ni}_{0.5}\text{Fe}_2\text{O}_4$  spinel nanostructures is also confirmed as the revealed diffraction peaks match both in intensity and the position of peaks in their standard diffraction pattern. However, there are two small peaks appear in the positions  $44.5^\circ$  and  $52^\circ$  for the powder samples as burnt at  $200^\circ\text{C}$ , which are belongs to the  $\text{Fe}_2\text{O}_3$  (maghemite) phase, and these two peaks will disappear with additional calcination of the samples at 400, 600 and  $800^\circ\text{C}$ .

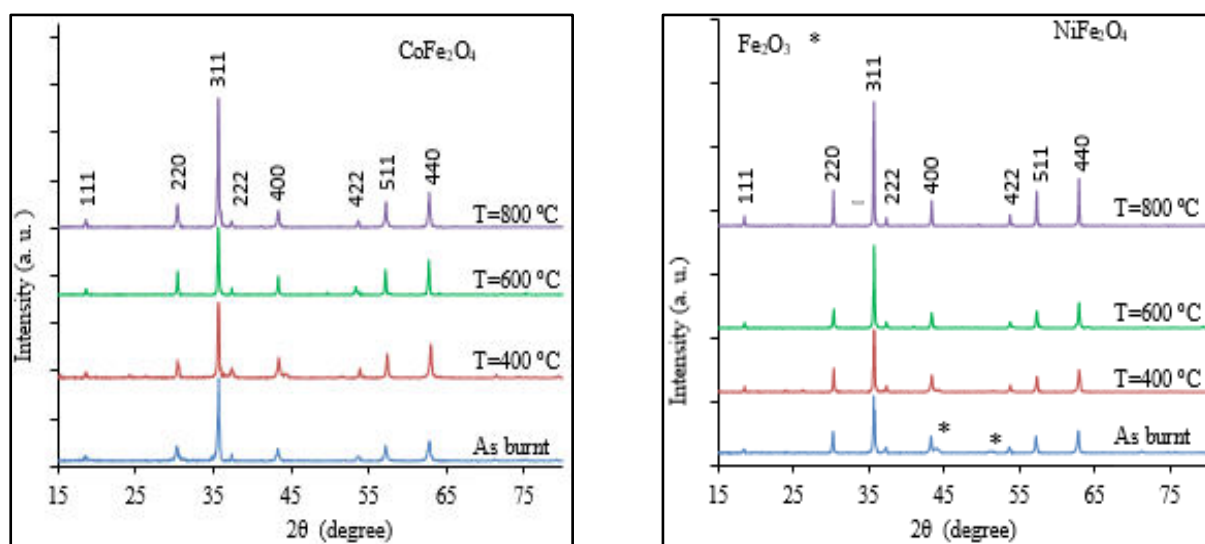


Fig. 3: X-ray diffraction patterns of the  $\text{CoFe}_2\text{O}_4$  ferrite NPs as-burnt and calcination at different temperatures. Fig. 4: X-ray diffraction patterns of the  $\text{NiFe}_2\text{O}_4$  ferrite NPs as-burnt and calcination at different temperatures.

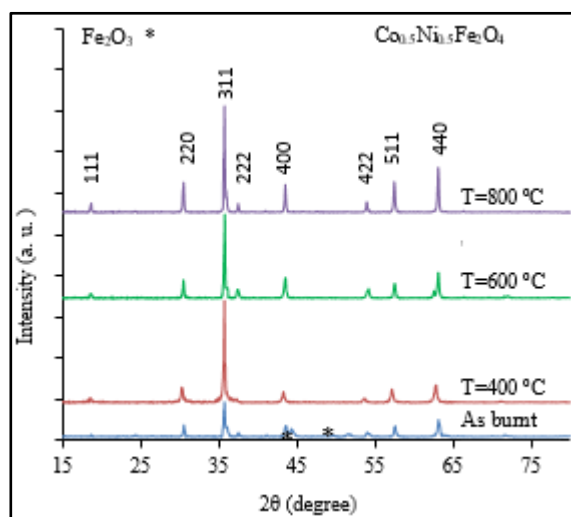


Fig. 5: X-ray diffraction pattern of  $\text{Co}_{0.5}\text{Ni}_{0.5}\text{Fe}_2\text{O}_4$  ferrite NPs as burnt and calcination at different temperatures.

The presence of maghemite is anticipated as annealing the samples at temperatures higher than  $180^\circ\text{C}$  will cause rapid oxidation of  $\text{Fe}^{+2}$  to  $\text{Fe}^{+3}$  which promotes formation of maghemite. The highest intensity of main peak (311) is appeared at  $800^\circ\text{C}$ .

Figure 6, shows the XRD patterns of the  $\text{Co}_{1-x}\text{Ni}_x\text{Fe}_2\text{O}_4$  ferrite nanopowders calcined at  $800^\circ\text{C}$  with different x

values (x= 0, 0.5 and 1). All pattern peaks are closely resembled the standard crystalline structure of Co-Ni ferrite from the International Centre for Diffraction Data (ICDD). In addition, the peak position of the XRD patterns does not alter after partial the substitution of Ni into the CoFe<sub>2</sub>O<sub>4</sub>. This is due to the comparatively same scattering factor of Co and Ni, as they are neighboring element in the periodic table and hence atomic positions are unchanged. This also gives the small reflection for 0.5 substitution of Ni. The small shift in the XRD patterns is observed at higher 2θ angle, when the Ni content in the product increases. This can be explained by the fact that the ionic radius (0.72 Å) of Ni<sup>+2</sup> ions is smaller than that (0.74 Å) of Co<sup>+2</sup> ions.

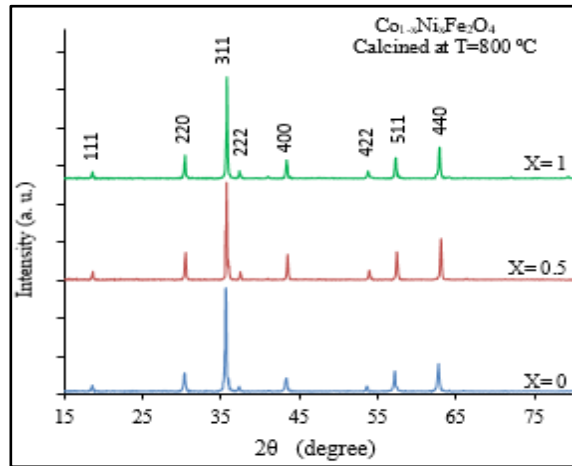


Fig. 6: X-ray diffraction pattern of Co<sub>1-x</sub>Ni<sub>x</sub>Fe<sub>2</sub>O<sub>4</sub> ferrite NPs calcined at 800C and with x= 0, 0.5 and 1.

From the XRD results, various structural parameters were calculated using standard relation as follows: Using the values of Bragg’s angle 2θ and interplanar spacing (d), the values of lattice constant (a) of nickel-Cobalt ferrite nano-particles was calculated using the following relation [31],

$$a = d \sqrt{h^2 + k^2 + l^2} \text{ \AA} \dots\dots\dots (1)$$

where the parameters h, k and l are represents the miler indices. The interplanar spacing d is calculated by using the Bragg law of XRD, as:

$$n \lambda = 2d \sin\theta \dots\dots\dots (2)$$

where, (n)is the order of diffraction, (λ) is the wavelength of the X-ray employed are equals to 1.54056Å for the Cu-Kα, source and (θ)is Bragg’s angle.

The crystallite size (t) of the Co-Ni ferrite nanoparticles was calculated from the main peak (311) in the XRD patterns using the Debbye-Scherer’s equation [32],

$$t = \frac{k\lambda}{\beta \cos\theta} \text{ nm} \dots\dots\dots (3)$$

where, k is Scherer’s constant and equals to (0.89) for spinel ferrite, (β)is the full width at half maximum (FWHM) of the peak (311) recorded XRD pattern, taken in radians. A semi-empirical relationship using to estimate the surface area of these nanoparticles by the following equation [33],

$$SSA = \frac{6000}{t d_x} \text{ (m}^2\text{/g)} \dots\dots\dots (4)$$

The dislocation density (δ) of nickel ferrite nanoparticles was calculated using the equation given by,

$$\delta = \frac{1}{t^2} \text{ line / m}^2 \dots\dots\dots (5)$$

The lattice strain (ε) was calculated using formula (34),

$$\epsilon = \frac{\beta}{4 \tan \theta} \dots\dots\dots (6)$$

The X-ray density (d<sub>x</sub>) of the ferrite nanoparticles was calculated using the equation given by,

$$d_x = 8 M / a^3 N_A \text{ ( g/cm}^3\text{)} \dots\dots\dots (7)$$

Where, ( $M$ ) is the molecular weight of the composition, ( $N_A$ ) is the Avogadro number and ( $a$ ) is the lattice constant. ( $L_A$ ) and ( $L_B$ ) is determined from the following relations [35]:

$$L_A = 0.25 a \sqrt{3}, \quad L_B = 0.25 a \sqrt{2} \dots\dots (8)$$

Where, ( $L_A$ ) and ( $L_B$ ) denoted to the hopping length for A- and B –sites, respectively.

All X-ray characteristic parameters of the  $Co_{1-x}Ni_xFe_2O_4$  spinel ferrite nanoparticles calcined at different temperatures (as-burnt, 400, 600 and 800 °C) are listed in the table (1), and were calculated using the standard relations shown in equations (1-8), Respectively.

**X-ray parameters as a function of calcination temperatures**

The XRD parameters of the  $Co_{1-x}Ni_xFe_2O_4$  ferrite nanoparticles calcined at different temperatures (as burnt 200, 400, 600 and 800°C). Figure (6) show that the crystallite size ( $t$ ) of the Co- and Ni- ferrites are increases in the range of (29-44 nm) and (27-39 nm) with increasing the calcination temperatures, respectively. In addition, the lattice constant ( $a$ ) of the Co- and Ni- ferrites increases in the range of (8.364-8.374 Å) and from (8.325-8.336 Å) respectively, these are consistent with the previous results report [36]. As the calcination temperature increases, the peaks become sharp reflects improved crystallite size and crystallinity, while the variations of the lattice constant are due to the different ionic radii,  $Ni^{+2}$  (tetrahedral 0.58; octahedral 0.69 Å) and  $Co^{+2}$  (tetrahedral 0.58; octahedral 0.74Å) [37].

Table 1: X-ray parameters;  $t$  (crystallite size),  $a$  (lattice constant),  $d_x$  (x-ray density),  $L_A$ ,  $L_B$  (hopping length for tetrahedral and octahedral sites respectively),  $\epsilon$  (Lattice strain), SSA (Specific Surface Area), and  $\delta$  (dislocation density) for Co-Ni ferrites at different temperatures

Spinel ferrite	Calcination temperature (°C)	2θ (degree) Peak (311)	Crystallite size t (nm)	lattice constant a (°A)	X-ray density $d_x$ (g/cm <sup>3</sup> )	hopping Length $L_A$ (°A)	hopping Length $L_B$ (°A)	dislocation density $\delta \times 10^{14}$ (line/m <sup>2</sup> )	Lattice strain $\epsilon \times 10^{-3}$	Specific surface area SSA (m <sup>2</sup> /g)
CoFe <sub>2</sub> O <sub>4</sub>	As-burnt	35.780	29.530	8.364	5.325	3.622	2.957	11.467	3.82	38.15
	400	35.774	36.240	8.369	5.317	3.624	2.959	7.614	3.12	31.14
	600	35.779	40.228	8.372	5.311	3.625	2.960	6.179	2.81	28.08
	800	35.763	44.356	8.374	5.307	3.626	2.961	5.083	2.55	25.49
NiFe <sub>2</sub> O <sub>4</sub>	As-burnt	35.716	27.423	8.325	5.396	3.605	2.943	13.298	4.12	40.55
	400	35.682	32.237	8.328	5.390	3.606	2.944	9.622	3.51	34.53
	600	35.688	35.863	8.332	5.383	3.608	2.946	7.775	3.16	31.08
	800	35.683	38.994	8.336	5.374	3.610	2.947	6.577	2.90	28.63
Co <sub>0.5</sub> Ni <sub>0.5</sub> Fe <sub>2</sub> O <sub>4</sub>	800	35.758	41.139	8.353	5.345	3.617	2.953	5.909	2.75	27.29

The increase of the lattice constant with calcination temperatures led to a decrease in the lattice compaction, and as a result, we obtained a decrease in the x-ray density and the dislocation density with the increasing the calcination temperature as illustrated in Figure 7. X-ray density and dislocation density values are in the table (1), while it was noted that nickel ferrite has higher values of x-ray density and dislocation density than that of cobalt ferrite and this is due to the lower lattice parameters of nickel ferrite

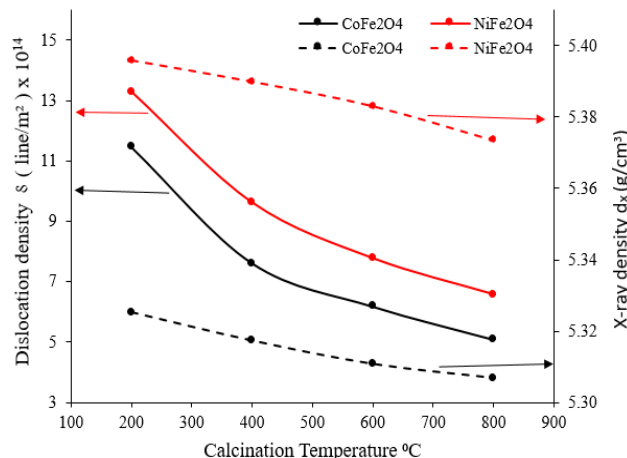
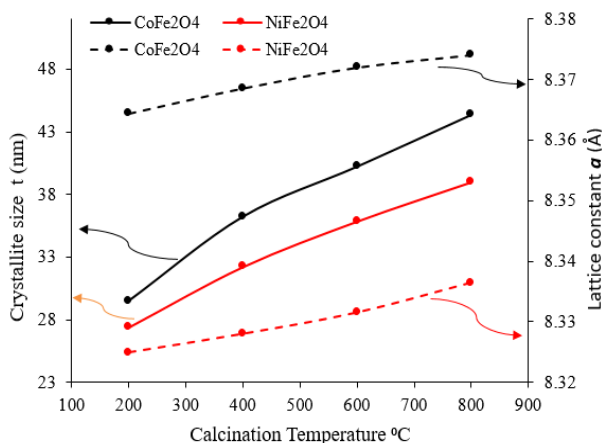


**Fig. 6: Crystallite size and lattice constant versus calcined temperatures for Co- and Ni-ferrite nano particles**      **Fig. 7: X-ray density and dislocation density versus calcined temperatures for Co- and Ni-ferrite nano particles**

Figure (8) shows that the hopping lengths of octahedral is larger than that of tetrahedral for Ni- and Co-ferrites, while the octahedral and tetrahedral hopping lengths of the Co-ferrite are greater than that of Ni-ferrite and they increases with increasing the calcination temperatures. All these differences in the hopping length, which depend on the temperature and the type of ferrite, are due to the different ionic radii, Ni<sup>+2</sup> (tetrahedral 0.58; octahedral 0.69 Å) and Co<sup>+2</sup> (tetrahedral 0.58; octahedral 0.74Å).

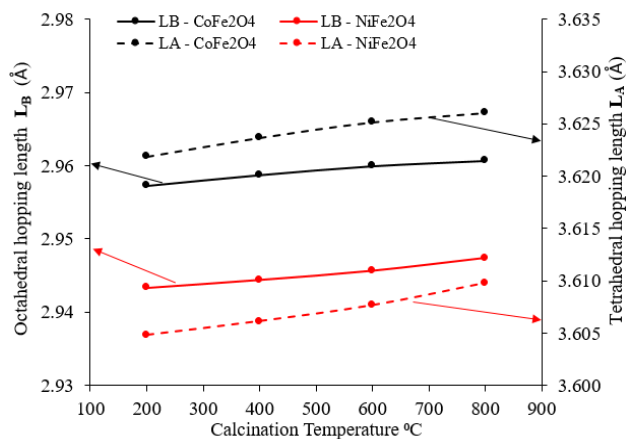


**Fig. 8: Hopping length L<sub>A</sub> and L<sub>B</sub> versus calcined temperatures for Co- and Ni-ferrite nano particles.**

The lattice strain is induced during the calcination process. Figure (9) shows that the lattice strain decreases with increasing the calcination temperature for the Co- and Ni-ferrites due to the increase in crystallite size during the calcination process, which in turn leads to a decrease in the lattice strain with increasing temperatures. As a result of the fact that the crystallite size of nickel ferrite is smaller than that of cobalt ferrite, the lattice strain of nickel ferrite is greater than that of cobalt ferrite.

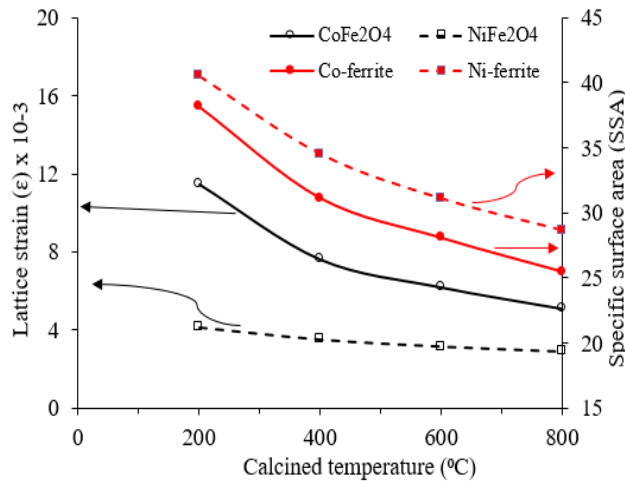


Fig. 9: Lattice strain versus calcined temper-atures for Co- and Ni-ferrite nano particles.

**X-ray parameters as a function of Ni-ion Concentration**

The substitution of the smaller Ni<sup>+2</sup> (0.72 Å) instead of the Co<sup>+2</sup> (0.74 Å) in Co<sub>1-x</sub>Ni<sub>x</sub>Fe<sub>2</sub>O<sub>4</sub> ferrite calcined at temperature of 800°C will greatly affect the XRD parameters, and the figures (10)-(13) are combined with Table (1) that shows this in detail.

Variation of crystallite size, lattice constant, and Hopping lengths parameters with Ni-ion concentration are shown in Figures (10) and (11). At a fixed Calcination temperature 800°C, these parameters are decreases with increasing Ni-ion concentration due to the difference in the ionic radii in tetrahedral and octahedral sites while, the value of these parameters ate listed in table (1).

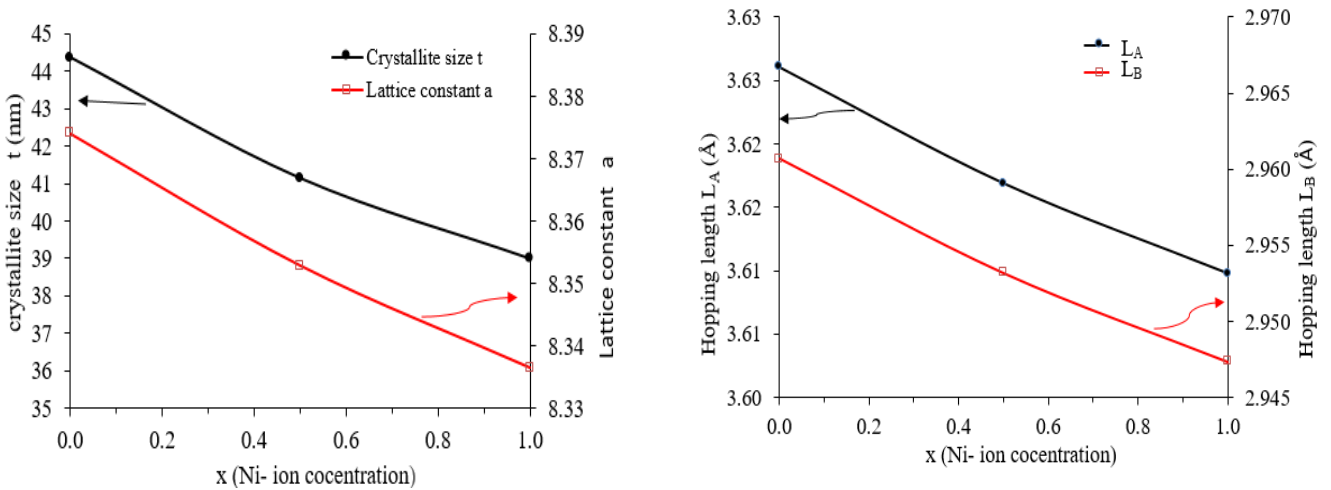
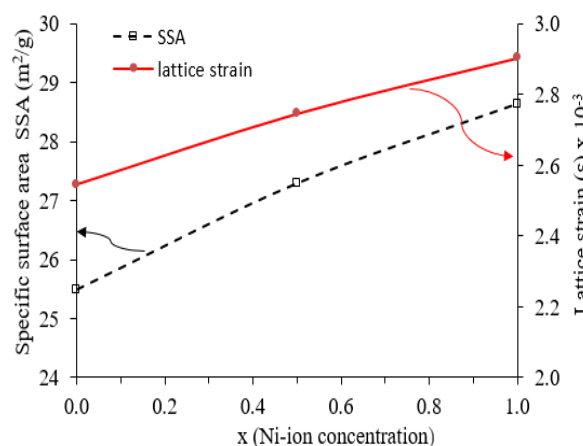
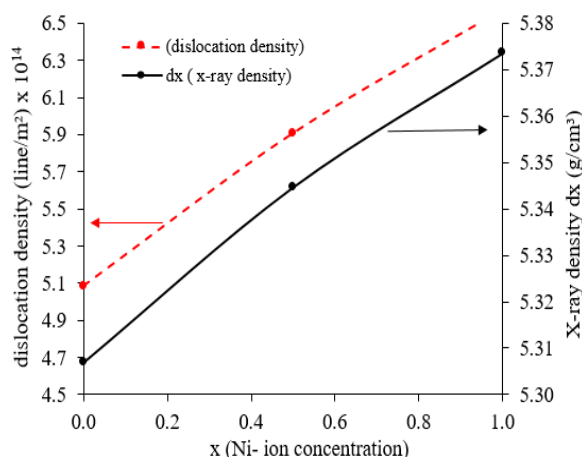


Fig. 10: Crystallite size and lattice constant versus Ni-ion concentration of Co<sub>1-x</sub>Ni<sub>x</sub>Fe<sub>2</sub>O<sub>4</sub> calcined at 800°C. Fig.11: Hopping length L<sub>A</sub> and L<sub>B</sub> versus Ni-ion concentration of Co<sub>1-x</sub>Ni<sub>x</sub>Fe<sub>2</sub>O<sub>4</sub> calcined at 800 °C.

The structural parameters illustrated in figures (12) and (13); X-ray density, dislocation density, Lattice strain and specific surface area are increases with increasing Ni-ion concentration in Co<sub>1-x</sub>Ni<sub>x</sub>Fe<sub>2</sub>O<sub>4</sub> ferrite calcined at fixed temperature of 800°C. Because of the lattice constant decreasing with increasing Ni- ion concentration in ferrite calcined at 800°C, the lattice strain will increase because the surface area for interaction becomes smaller increasing the lattice strain. Whereas, replacing the Co-ions with smaller Ni-ions in cobalt ferrite structure leads to the formation of a compact crystal, which causes an increase in the x-ray density. The dislocation density and specific surface area are inversely proportional to the crystallite size, so replacing cobalt ferrite with smaller ions will lead to

a smaller crystal size and thus result in an increase in dislocation density and specific surface area.



**Fig. 12: x-ray density and dislocation density versus Ni-ion concentration of  $Co_{1-x}Ni_xFe_2O_4$  calcined 800 °C.** **Fig. 13: Lattice strain versus Ni-ion concentration of  $Co_{1-x}Ni_xFe_2O_4$  calcined at 800 °C.**

### Electron Scanning Microscope (SEM)

Morphology of the synthesized  $CoFe_2O_4$ ,  $NiFe_2O_4$ , and  $Co_{0.5}Ni_{0.5}Fe_2O_4$  spinel ferrite nanopowders by sol-gel autocombustion method was investigate using scanning electron microscope (SEM). The scanning electron microscopic images of all the prepared powders were illustrate in Figure (14).

The formation of particles that have an almost homogeneous distribution with semi-spherical form and some of them are in the agglomerated form in  $CoFe_2O_4$ ,  $NiFe_2O_4$ , and  $Co_{0.5}Ni_{0.5}Fe_2O_4$  nanopowders is very clear in SEM images provided in Figure (14). The microscopic images confirm that the nanoparticles formed in  $NiFe_2O_4$  ferrite are smaller than the nanoparticles in  $CoFe_2O_4$  ferrite, while the particles formed in  $Ni_{0.5}Co_{0.5}Fe_2O_4$  ferrite are of intermediate sizes. The sizes of the particles in the  $CoFe_2O_4$ ,  $NiFe_2O_4$ , and  $Co_{0.5}Ni_{0.5}Fe_2O_4$  powders varied in the range of (45-53 nm), (39-47 nm), and (41-48nm), respectively. The size variation observed for the particles is in good agreement with their average crystallite sizes determined from XRD spectra (as shown in table 2). Therefore, the  $CoFe_2O_4$  NPs formed at a considerably faster growth rate than the  $NiFe_2O_4$  NPs prepared at the calcination temperature of 800 °C for 3 hours used in the present work.

**Table 2: average particle size ( $t_{SEM}$ ) and average crystallite size ( $t_{XRD}$ ) for  $CoFe_2O_4$ ,  $Co_{0.5}Ni_{0.5}Fe_2O_4$  and  $NiFe_2O_4$  calcined at temperature 800 °C for 3 h.**

Ferrite	Average particle size ( $t_{SEM}$ ) nm	Average Crystallite size ( $t_{XRD}$ ) nm
$CoFe_2O_4$	45-53	42-45
$Co_{0.5}Ni_{0.5}Fe_2O_4$	41-48	40-42
$NiFe_2O_4$	39-47	39-41

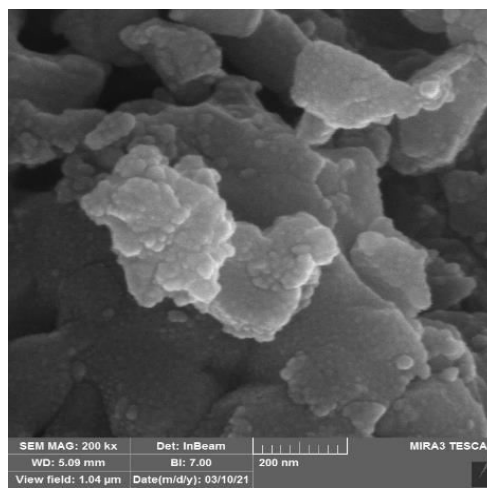
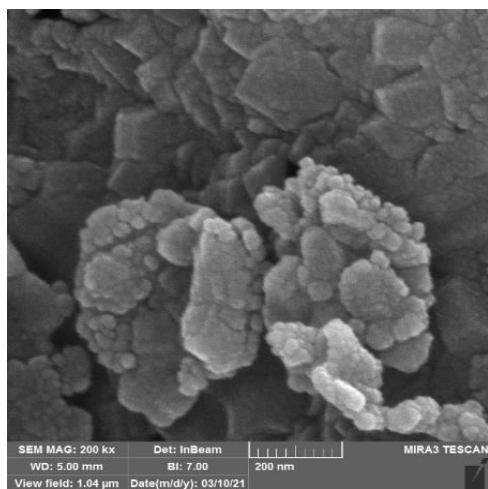


Figure 15 (a): SEM images of CoFe<sub>2</sub>O<sub>4</sub>, ferrite nanoparticles for calcined samples at 800°C.

Figure 15 (b): SEM images of Co<sub>0.5</sub>Ni<sub>0.5</sub>Fe<sub>2</sub>O<sub>4</sub> ferrite nanoparticles for calcined samples at 800°C.

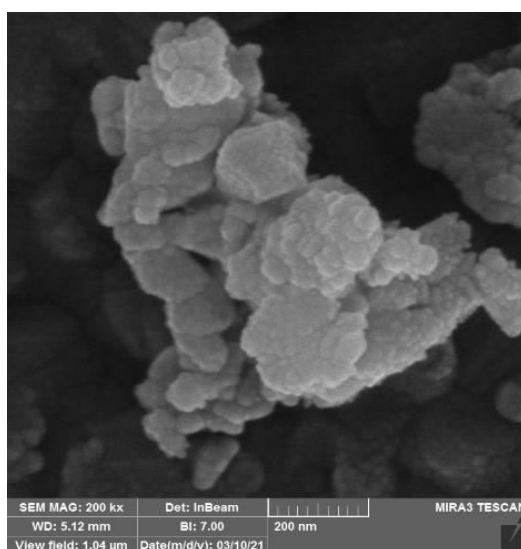


Figure 15 (c): SEM images of NiFe<sub>2</sub>O<sub>4</sub>, ferrite Nano-powders for calcined samples at 800°C.

## Conclusions

Cobalt-Nickel ferrite nanopowders with chemical formula of Co<sub>1-x</sub>Ni<sub>x</sub>Fe<sub>2</sub>O<sub>4</sub> (where, x= 0.0, 0.5, 1.0) were successfully synthesized using sol-gel auto combustion method and calcined at temperatures (as-burnt, 400, 600, 800°C). The effect of calcination temperature on crystallinity, phase composition and morphology was investigated by various characterization methods, i.e., XRD and SEM respectively. XRD displayed that all samples exhibited the characteristic behavior of cubic spinel ferrite nanoparticle. The crystallite size, lattice parameter, x-ray density, dislocation density, lattice strain, specific surface area and hopping lengths were found to be dependent on the Ni-ion concentration and calcination temperatures. SEM images clearly showed that the crystallite size (depends on the XRD) and particle size (depends on the SEM) increases as the calcination increases, while they decrease as the Ni-ion concentration increases.

**References**

- [1] Ahsan, M. Z., Islam, M.A., Bally, A.A., and Khan, F.A. Spectroscopic analysis for electric and magnetic properties of manganese doped cobalt nanoferrite, *Results in Physics*, Vol. 17, pp. 1-10, June 2020.  
<https://doi.org/10.1016/j.rinp.2020.103172>
- [2] Dippong, T., Levei, E. A., and Cadar, O., Recent Advances in Synthesis and Applications of  $MFe_2O_4$  (M= Co, Cu, Mn, Ni, Zn) Nanoparticles, *Nanomaterials*, Vol. 11, pp. 1-33, 2021.  
<https://doi.org/10.3390/nano11061560>
- [3] Sharma, S., Daya, K., Sharma S., and Singh, M., Ultra low loss soft magnetic nanoparticles for applications up to S-band, *Applied Physics Letters*, Vol. 103, Issue 11, 112402 (2013) <https://doi.org/10.1063/1.4820916>
- [4] Houbi, A., Aldashevich, Z. A., and Atassi, Y. Microwave absorbing properties of ferrites and their composites: A Review, *Journal of Magnetism and Magnetic Materials*, Vol. 529 No.14:167839  
DOI: 10.1016/j.jmmm.2021.167839
- [5] S. M. Hussein, T.H. Mubarak, S.M. Ali Ridha, and J. Al-Zanganawee. Synthesis and Studying Induction Heating of  $Mn_{1-x}Zn_xFe_2O_4$  ( $x=0-0.5$ ) Magnetic Nanoparticles for Hyperthermia Treatments, *Key Engineering Materials*, Vol. 882, pp. 200-218, April 2021.  
[doi.org/10.4028/www.scientific.net/KEM.882.200](https://doi.org/10.4028/www.scientific.net/KEM.882.200)
- [6] Rathore, D., Kurchania, R., and Pandey, R., Gas Sensing Properties of Size Varying  $CoFe_2O_4$  Nanoparticles, *IEEE Sensors Journal*, Vol. 15, No. 9, Pp. 4961-4966, September 2015  
DOI: 10.1109/JSEN.2015.2432035
- [7] González-Martín, R., Gutiérrez-Serpa, A., and Pino, V. The Use of Ferro fluids in Analytical Sample Preparation: A Review, *Separations*, Vol. 8, No. 47, Pp. 1-14, 2021.  
<https://doi.org/10.3390/separations8040047>
- [8] Boris, I. K., Diasb, H. V. and Kharissova O. V. Mini-review: Ferrite nanoparticles in the catalysis, *Arabian Journal of Chemistry*, Vol. 12, Issue 7, Pages 1234-1246, November 2019.  
<https://doi.org/10.1016/j.arabjc.2014.10.049>
- [9] Kasinathan, K., Kennedy, J., Elayaperumal, M., Henini, M., and Malik, M., Photo-degradation of organic pollutants RhB dye using UV simulated sunlight on ceria based  $TiO_2$  nanomaterials for antibacterial applications, *Scientific reports*, 6(38064), 2016. DOI: 10.1038/srep38064
- [10] Raghvendra, S. Yadav, J., and et. al., Impact of  $Nd^{3+}$  in  $CoFe_2O_4$  spinel ferrite nanoparticles on cation distribution, structural and magnetic properties, *Journal of Magnetism and Magnetic Materials*, Vol. 399, Pp. 109-117, (2016).  
<https://doi.org/10.1016/j.jmmm.2015.09.055>.
- [11] Pramanik, N.C., Fujii, T., Nakanishi, M., and Takada, J. Effect of  $Co^{2+}$  ion on the magnetic properties of sol-gel cobalt ferrite thin films, *Journal of Materials Chemistry*, Vol. 14, Pp. 3328-3332, (2004).  
<https://doi.org/10.1039/B410163D>
- [12] Reddy, D. H. K., and Yun, Y.-S., Spinel ferrite magnetic adsorbents: Alternative future materials for water purification, *Coordination Chemistry Reviews*, Vol. 315, Pp. 90-111, (2016).  
<https://doi.org/10.1016/j.ccr.2016.01.012>.
- [13] Kombaiyah, K., Vijaya, J.J., and et. al., Comparative investigation on the structural, morphological, optical, and magnetic properties of  $CoFe_2O_4$  nanoparticles, *Ceramics International*, Vol. 43, No. 10, pp. 7682-7689, (2017).  
DOI: 10.1016/j.ceramint.2017.03.069.
- [14] Malinowska, I., and et. al., Synthesis of  $CoFe_2O_4$  Nanoparticles: The Effect of Ionic Strength, Concentration, and Precursor Type on Morphology and Magnetic Properties, *Research Article*, Volume 2020 |Article ID 9046219 | <https://doi.org/10.1155/2020/9046219>.
- [15] Hochepeid, J., Bonville, P., and Pileni, M., Nonstoichiometric Zinc Ferrite Nanocrystals: Synthesis and Unusual Magnetic Properties. *Journal of Physical Chemistry B*. Vol. 104, No. 5, Pp. 905-912, 2000.  
DOI:10.1021/JP991626I
- [16] Liu C, Zou B, Rondinone AJ, Zhang ZJ. Reverse micelle synthesis and characterization of superparamagnetic  $MnFe_2O_4$  spinel ferrite nanocrystallites. *Journal of Physical Chemistry B*. 2000;104(6):1141-1145.
- [17] Chen, Ch., Jianfeng, D., Zengpeng, L. and Wei F., Preparation and Magnetic Properties of  $CoFe_2O_4$

- Oriented Fiber Arrays by Electrospinning, *Materials*, Vol. 13, Pp. 1-11, 3860, 2020.  
doi:10.3390/ma13173860.
- [18] Shi, Y., Ding, J., and Yin, H. CoFe<sub>2</sub>O<sub>4</sub> nanoparticles prepared by the mechanochemical method. *Journal of Alloys and Compounds*, Vol. 308, No. (1-2), Pp. 290-295, 2000.  
DOI: 10.1016/S0925-8388(00)00921-X
- [19]. Maaz, K., Khalid, W., Mumtaz, A., Hasanin, S., Liu, J., and Duan, J., Magnetic characterization of Co<sub>1-x</sub>Ni<sub>x</sub>Fe<sub>2</sub>O<sub>4</sub> (0≤x≤1) nanoparticles prepared by co-precipitation route. *Physica E: Low-dimensional Systems and Nanostructures*, Vol. 41, No. 4, Pp. 593-599, 2009
- [20]. Sirvetz M.H., and Saunders, J.H. Resonance widths in polycrystalline nickel-cobalt ferrites. *Physical Review*, Vol. 102, No.2, Pp. 366-367, 1956.
- [21]Naresh, U., Kumar, J., and Naidu, K., Hydrothermal synthesis of barium copper ferrite nanoparticles: Nanofiber formation, optical, and magnetic properties, *Materials Chemistry and Physics*, Volume 236, 1 October 2019.  
doi.org/10.1016/j.matchemphys.2019.121807
- [22]Muniba, M. K., and et. al., Aluminum Substitution in Ni-Co Based Spinel Ferrite Nanoparticles by Sol-Gel Auto-Combustion Method, *Journal of Electronic Materials*, volume 50, pages3302–3311 (2021).
- [23]Nining, S. A., Awan M., and Nesya, I. B., Synthesis and Characterization of Soft Magnetic Materials Ni<sub>x</sub>Zn<sub>1-x</sub>Fe<sub>2</sub>O<sub>4</sub> (x = 0,2 – 0,8) Lombok Iron Sand with Co-precipitation Method, *Journal of Technomaterials Physics* Vol. 03, No. 01, pp. 21-28, 2021  
<https://talenta.usu.ac.id/JoTP>
- [24]Tahir, M. B., Tahir, L., Ali, H., and Snobia, G. Wet Chemical Co-precipitation Synthesis of Nickel Ferrite Nanoparticles and Their Characterization, *Journal of Inorganic and Organometallic Polymers and Materials*, Vol. 27, no. 5, pp. 1430-1438, September 2017  
DOI 10.1007/s10904-017-0598-5
- [25] Chen L, Dai H, Shen Y, Bai J. Size-controlled synthesis and magnetic properties of NiFe<sub>2</sub>O<sub>4</sub> hollow nanospheres via a gel-assistant hydrothermal route. *Journal of Alloys and Compounds*. 2010;91(1-2):L33-L38.  
[ [Links](#) ]
- [26] [22] Sivakumar P, Ramesh R, Ramanand A, Ponnusamy S, Muthamizhchelvan C. Preparation of sheet like polycrystalline NiFe<sub>2</sub>O<sub>4</sub> nanostructure with PVA matrices and their properties. *Materials Letters*. 2011;65(9):1438-1440. [ [Links](#) ]
- [27] Darshane, S.L., Deshmukh, R.G., and et. al. Gas-sensing properties of zinc ferrite nanoparticles synthesized by the molten-salt route, *Journal of the American Ceramic Society*, Vol. 91, No. 8, pp. 2724-2726, 2008
- [28] Mathew, D.S. and Juang, R.S. An Overview of the Structure and Magnetism of Spinel Ferrite Nanoparticles and Their Synthesis in Microemulsions. *Chemical Engineering Journal*, Vol. 129, Pp. 51-65, 2007.  
<http://dx.doi.org/10.1016/j.cej.2006.11.001>
- [29] Zhang, R., Huang, J., Zhao, J., Sun, Zh., and Wang, Y., Sol-Gel Auto-Combustion Synthesis of Zinc Ferrite for Moderate Temperature Desulfurization, *Energy and Fuels*, Vol. 21, No. 5, pp. 2682-2687, 2007.  
DOI: 10.1021/ef070064w
- [30] Manish, S., Chaubey, S. and Animesh, K.O., Investigation on Size Dependent Structural and Magnetic Behavior of Nickel Ferrite Nanoparticles Prepared by Sol-Gel and Hydrothermal Methods, *Materials Chemistry and Physics*, Vol. 118, No. 1, pp. 174-180, 2009.  
DOI: 10.1016/j.matchemphys.2009.07.023
- [31] Kumari, M., and Bhatnagar, M. C. Synthesis of nickel ferrite nanorods and nano octahedrons by hydrothermal method. In *AIP Conference Proceedings*, Vol. 2220, No. 1, p. 110042). (2020, May). AIP Publishing LLC.
- [32] Patil, V., Shirsath, S.E., More, S., Shukla, S., and Jadhav, K. Effect of zinc substitution on structural and elastic properties of cobalt ferrite, *Journal of Alloys and Compounds*, Vol. 488, pp. 199- 203 (2009).
- [33] Pottker, W. E., Ono, R., and et., Influence of order-disorder effects on the magnetic and optical properties of NiFe<sub>2</sub>O<sub>4</sub> nanoparticles, *Ceramics International*, Volume 44, Issue 14, pp. 16103-17576, October 2018.
- [34] Sharma, K, and Sharma, P., impurity effect of La on Co ferrite: synthesis and structural study, *Optoelectronics and advanced materials-rapid communications*, vol. 7, No. 11-12, pp. 887-890, 2013.
- [35] Globus, A., Pascard, H. and Cagan, V., Distance between magnetic ions and fundamental properties in ferrites,

Journal de Physique, Vol. 38, No. C1, Pp. 163–168, 1977

[36] Pumama, B., Khoiriah, A., and Suharyana, Structural and magnetic properties of aluminium-substituted cobalt ferrite nanoparticles by the coprecipitation route. *Journal of Magnetism*, Vol.23, No. 1, pp. 106-111, 2018.

[37] Ashour, A.H., El-Batal, A.I., AbdeMaksoud, M.I.A., El-Sayyad, G.S., Labib, S., Abdeltwab, E., and El-Okr, M.M. Antimicrobial activity of metal-substituted cobalt ferrite nanoparticles synthesized by sol-gel technique. *Particuology*, Vol. 40, Pp. 141–151, 2018.

doi: 10.1016/j.partic.2017.12.001